Catalysis Science & Technology

Accepted Manuscript

ROYAL SOCIETY OF CHEMISTRY

www.rsc.org/catalysis

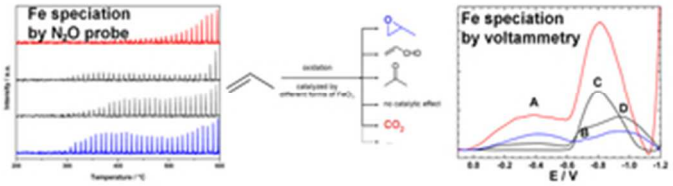

14x3mm (600 x 600 DPI)

Gas-phase epoxidation of propylene over iron-containing catalysts: the effect of iron incorporation in the support matrix

Blažej Horváth[a*], Martin Šustek[a], Ivo Vávra[c,e], Matej Mičušík[d], Miroslav Gál[b] and Milan Hronec[a*]

[a]Department of Organic Technology, [b]Department of Inorganic Technolgy, Slovak University of Technology, Radlinského 9, 81237 Bratislava, Slovak Republic

[c]Institute of Electrical Engineering, [d]Polymer Institute, Slovak Academy of Sciences, Dúbravská cesta 9, 84104 Bratislava, Slovak Republic,

[e]Nanotechnology Centre, VŠB-Technical University of Ostrava, 17.listopadu 15/2172, 70833 Ostrava-Poruba, Czech Republic

Abstract

The gas-phase epoxidation of propylene, using iron as a catalytically active metal have been studied. The XRD-amorphous silica nano-powder was found to host active as well as redox-silent iron species, using nitrous oxide as an oxidizing agent. A presence of iron oxide nanoparticles was proven in the most active catalysts, indicating that the epoxidation proceeds over nanoparticles, rather than over isolated iron atoms. A combination of XPS, TEM and voltammetirc techniques elucidated the mechanism of the formation of catalytically active forms of iron oxide, distinguishing selective forms from unselective and inactive ones in the epoxidation reaction. Transition-response experiments showed a good correlation between epoxidation activity, N_2O decomposition and electrochemical specification of iron oxides.

Keywords: propylene epoxidation, iron oxide nanoparticles, N_2O, electrochemical characterization, transition-response experiments

*corresponding authors, e-mail: blazej.horvath@stuba.sk (B.Horvath), milan.hronec@stuba.sk (M.Hronec)

1. Introduction

Propylene oxide (PO), one of the fifty most important intermediates in the chemical industry, is mainly consumed for the production of polyurethanes, cosmetics, pharmaceuticals, detergents, textiles, etc.[1] PO is industrially produced by the chlorohydrin and hydroperoxide processes. The chlorohydrin process, due to the usage of hazardous chlorine and the production of chlorinated organic by-products and the brine containing calcium chloride, suffers form environmental drawbacks [2]. About 60 % of the global PO production (9 mil. tons [3]) is based on hydroperoxide processes [4]. Widely used hydroperoxide processes produce fixed amounts of styrene or t-butyl alcohol co-products, causing separation problems and difficulties in balancing the markets for PO and the co-products [5]. Lately, alternative routes have been commercialized to address these problems, one example of them being the combination of the cumene hydroperoxide process, well known for the production of phenol, and a hydroperoxidation route to produce PO [6]. Recently, the epoxidation of propylene with hydrogen peroxide to PO (HPPO process) catalyzed by titanosilicates TS-1 has been introduced by Dow/BASF and Evonik/Uhde [7]. A disadvantage of the HPPO process, however, is the cost of the H_2O_2.

The direct gas-phase epoxidation of propylene to PO has been studied in recent years as an alternative route to industrial processes. Different oxidizing agents, including molecular oxygen [8], nitrous oxide [9, 10] as well as H_2-O_2 mixture [11,12] have been tested. Gold nanoparticles on TiO_2 were reported to catalyze propylene epoxidation using H_2-O_2 mixture with very high PO selectivity (>95 %) [13]. However, this catalytic system suffers from several drawbacks, as low propylene conversion and poor catalyst stability. Recently, the importance of the catalysts nanostructure for propylene epoxidation was repeatedly emphasized for various catalytic systems [14-16].

Although silver catalysts have been used for decades for ethylene epoxidation employing molecular oxygen, an analogy for propylene epoxidation seems to be much more challenging due to the reactivity of the allylic hydrogen in propylene molecule [17]. Hence, although molecular oxygen is a cheap and available oxidant, lower selectivities (<50 %) to PO with O_2 over Ag- and Cu- based catalysts were reported [18].

Nitrous oxide was reported as an outstandingly successful selective oxidizing agent, e.g. for the one-step hydroxylation of aromatics over Fe-ZSM-5 catalysts [19], for the oxydehydrogenation of propane to propylene [20] and for the oxidation of methane to methanol as well [21]. The epoxidation of propylene with N_2O had been reported using silica-supported iron oxide catalysts with 60% selectivity to PO at 6–12% propylene conversion [22]. For the same catalyst, a necessity of an alkaline acetate promoter have been deemed to attain the epoxidation activity, the effect of the promoter being mainly attributed to the neutralization of acidic sites on the catalysts surface, which are responsible for the combustion of propylene [23].

Recently, potassium halogenide promoted catalysts, involving modification by amines in preparation step, have shown 13.3% PO yield at 60% selectivity [24]. Hence, the necessity of the alkaline metal cation seems to be inevitable; however, the overall effect of the promoter is not yet sufficiently described. In the presence of calcium promoter, very high selectivity (96 %) to PO was achieved [9].

In the present work the interactions between the catalyst support, iron and promoters are investigated. The separate effects of the cation and anion of the promoter are discussed, in terms of the catalyst´s lifetime and selectivity toward PO. The distribution of the iron oxide nanoparticles in the support matrix, their specification by electochemical characterization and by specific reactivity to N_2O as a probe molecule are provided as well.

2. Experimental

2.1. Catalyst preparation and testing

Supported iron-containing catalysts were prepared by a wet impregnation technique, using an Aerosil 200® silica support (Degussa, with a declared specific surface area of 200 m^2g^{-1}). The parent catalyst, 1% FeO_X–30% KCl/SiO_2 (where FeO_X was calculated as Fe_2O_3), denoted as 1Fe-acac-Si-KCl (the first number denoting the concentration of deposited iron oxide in the final catalyst) was prepared by the impregnation of the support in concentrated aqueous solution of potassium chloride, depositing 30 wt.% of KCl. After evaporating of the water, the sample was finely crushed and dried at 200 °C. Then a 0.1% solution of iron

acetylacetonate (Fluka) in anhydrous toluene was added to the dry sample immediately. The solvent was evaporated under vacuum, and then the sample was calcined at 600°C for 5 h; a heating rate of 100 °C.h^{-1} was used. If not otherwise denoted, the catalyst samples were calcined in an air flow (70 ml.min^{-1}). To denote samples calcined in 5%H_2/N_2 or N_2 flow a specification *(H_2)* or *(N_2)* is added. The calcined samples were pelletized, crushed and sieved to a grain size of 0.1–0.3 mm. The samples denoted as 1Fe-phen-Si-KCl and 1Fe-bipy-Si-KCl were prepared accordingly, using Fe(III) tris(o-phenantroline) or Fe(III) tris(bipyridine) nitrates in methanolic solutions. Samples yFe-Cl-Si-KCl (where y denotes the iron content) were prepared by depositing the components $FeCl_3$ and KCl in one step from an aqueous solution. Samples yFe-NO_3-Si, yFe-form-Si, yFe-Cl-Si were prepared accordingly, using iron nitrate, formate and chloride precursors, respectively. 1Fe-CN-Si catalysts were prepared by using iron ferricyanide as an iron source together with tetraethyl orthosilicate (TEOS) in an acidic solution, using an Fe:Si:HCl:H_2O molar ratio 1:10:1:1000. Samples yFe-Cl-Si-KCl-NH_4Cl, yFe-acac-Si-KCl-NH_4Cl and yFe-acac-Si-KCl-KAc were prepared by substitution of 25% of the overall KCl by NH_4Cl or CH_3COOK, respectively.

The catalytic tests were carried out in a fixed-bed glass reactor, usually at a temperature 320 °C and atmospheric pressure, using 1 g of catalyst (with a grain size of 0.1–0.3 mm) and nitrous oxide as an oxidizing agent. A flow of 70 ml min^{-1} N_2O and 4 ml min^{-1} propylene was used. The temperature was controlled by the Fe–Ko thermocouple placed in the center of the catalyst bed. The catalysts were initially activated in an air flow (70 ml min^{-1}) at 550 °C for 30 min., then the temperature was decreased to 320 °C and the inlet gas was switched to N_2O. After 10 min. of equilibration, propylene was introduced. The reaction products were identified by a Shimadzu Pyr-GCMS-QP 2010 Ultra system, and analyzed by on-line GC, equipped with Porapak Q (for the analysis of the organic products) and Carbosieve (for CO and CO_2) columns and with FID and TCD detectors.

XPS patterns were recorded using a Thermo Scientific K-Alpha XPS system equipped with a micro-focused, monochromatic Al Kα X-ray source (1486.6 eV). All the samples were scanned three times, with a resulting accuracy of the XPS peak positions < ±0.1 eV. The N_2O decomposition measurements were carried out in a fixed-bed quartz reactor – using 300mg of catalyst sample 10 ml.min^{-1} of helium as a carrier gas – equipped on-line with a Shimadzu Pyr-GCMS-QP 2010 Ultra system. Voltammetric analysis was performed using a carbon paste

anode as a working electrode and a platinum mesh cathode. The catalyst sample was mechanically deposited on the surface of the working electrode. The voltammetric patterns were recorded using a Solartron SI 1287 potentiostat in an argon-purged acetate buffer (0.1 M acetic acid and 0.1M sodium acetate, pH=4.7), using a standard calomel reference electrode (SCE), according to the procedure described in [25]. For TEM imaging a JEOL 1200 EX microscope was used, at an accelerating voltage 120 kV.

3. Results

3.1 XPS-study

It had been previously found, that iron species located inside narrow pores are most likely to lead to the products of overoxidation of propylene due to propylene oxide being less stable at elevated temperatures that propylene itself [24]. Hence, the most suitable sites responsible for selective epoxidation are expected to be located near the outer surface, making a surface-sensitive XPS screening substantial.

As described in Chap. 3.5, the composition of the atmosphere during the catalyst calcination does alter the catalytic properties of the resulting sample.To test the effect of calcination atmosphere on the chemical composition of the catalysts´ surface, a pair of 1Fe-acac-Si-KCl samples, calcined in a flow of air, and N_2 , respectively, was prepared.

The XPS patterns of the samples prepared in inert (nitrogen) and oxidizing (air) atmosphere show several differences (Fig. 1):

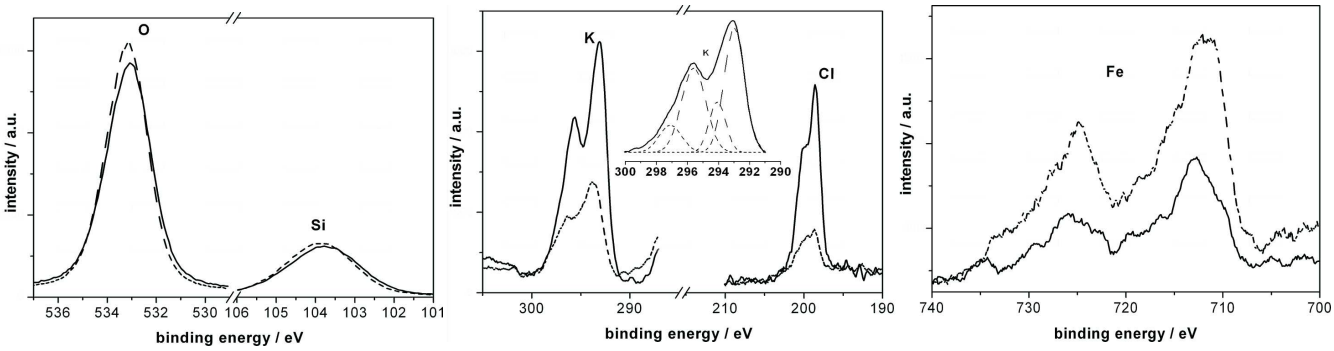

Fig.1.: XPS spectra of the 1Fe-acac-Si-KCl catalyst calcined in air (full line) and in nitrogen (dashed line). The patterns for Fe were smoothed using a Savitzky-Golay algorithm.

The theoretical molar concentrations for the precursor 1%wt.Fe_2O_3-30wt.%KCl/SiO_2 are: 26.8% Si, 54.1% O, 9.4% K, 9.4% Cl, 0.3% Fe. The surface concentration of silicon and oxygen, found by XPS were: 34.4 mol% silicon and 60.6 mol% oxygen for sample calcined in nitrogen, and 59.3 mol% O and 33.5% Si for the sample calcined in air, representing a Si/O ratio 1:1.76 and 1:1.77, respectively.

Surprisingly, the surface concentration of potassium chloride, detected by XPS, was much lower than the bulk KCl-content, only a small portion of KCl migrated to the external surface. The calcination in air has stronger influence on the migration of potassium chloride to the catalyst surface, increasing the potassium concentration on the surface from 0.5% for nitrogen-calcined sample to 1.7% for the air-calcined one. Another striking effect, a disbalance in the K/Cl ratio had been found, the K/Cl ratio being 0.71for the nitrogen-calcined sample and 0.81 for the air-calcined one. Thus, calcination of the catalyst in air – in comparison to nitrogen – leads to a surface richer in potassium and chlorine. Moreover, the calcination in air mitigates the deficit of surface chlorine, however, the deficit of chlorine still being significant. Hence, one should consider a chemical reaction involving the potassium chloride during the calcination, resulting in phases with a molar ratio of K/Cl different from that in KCl.

On the XPS patterns there are also slight shifts in the binding energies of silicon and oxygen, decreasing by 0.1-0.2 eV for both elements upon air activation. SiO_2 can interact only with potassium, chlorine and iron – the elements present in the catalyst –, what necessitates the formation of silicates, documented in the decrease in the binding energies for Si and O. The formation of silicates is apparently more distinctive for the sample calcined in air.

As the binding energies for silicon and oxygen decreased slighly upon calcination in air (indicating a reaction with the potassium cation resulting in the formation of silicates), there should be markedly a corresponding shift also for potassium. While for the majority of elements an oxidation (or a proximity of an electron acceptor) leads to an increase in the binding energies in XPS, some alkaline metals represent a known exception. For the potassium an increase in binding energy indicates reducion or a loss of an electronegative counterpart (e.g. halogenide ion). Hence, a transformation of potassium chloride into silicates should bring about an appearance of a peak for K at higher binding energies. A shoulder of K-peak, observed in the XPS pattern of the air-activated catalyst at 297.4 eV indicates the presence of a part of the potassium being bind in a silicate form. Hence, after the calcination of the catalyst in air, there

is dominantly potassium chloride present on the surface, together with a smaller portion of silicates. Upon calcination in nitrogen a transformation of silicon oxide to silicates takes place in smaller extent (as documented by the shifts of Si and O to lower binding energies); however, the transformation of potassium chloride to silicates occurs in greater extent (evident form onset of the potassium peak being shifted to higher values in the nitrogen-calcined sample). This is only possible when the extent of the migration of KCl to the surface upon air activation overwhelms that of the silicate formation, while during calcination in nitrogen the formation of silicates dominates.

A slight increase in the binding energy of iron after calcination in air, indicating its oxidation, is not surprising. However, along with the migration of the chlorine during the calcination in air, we can observe a deterioration of the surface iron content, from 0.4% for nitrogen-calcinated sample to 0.2% for sample calcined in air.

One of the most critical aspects, reported for iron-containing catalysts applied in oxidation reactions is the amount of iron introduced into the catalyst during its preparation. It had repeatedly been remarked that the increasing concentration of iron in a catalyst usually leads to a loss of selectivity [26, 27]. Some previously reported tools to enhance the incorporation of iron into the silica-based matrix – alongside with the well-known steaming procedure used for Fe-containing zeolites [26] – were e.g. the utilization of promoters, the optimization of the calcination conditions, or the choice of a support with a suitable texture [22-24].

On a silica support, we can observe remarkable differences in the XPS-patterns of the catalysts when using ferricyanide and chloride-based iron precursors. When comparing the XPS-patterns of the catalysts 1Fe-CN-Si and 6Fe-Cl-Si-KCl calcined in air flow, we can see that in spite of the significanty different bulk iron content (1% and 6%), in both catalysts there is practically the same iron concentration on the surface (0.41 % in the 1Fe-CN-Si and 0.38% in the 6Fe-Cl-Si-KCl catalyst) (see Fig. 2). These concentrations are well below the expected bulk level. Another information, recoverable form the Fe-signals of the above mentioned catalysts, is that for iron there is no observable difference in the binding energies between the 1Fe-CN-Si and 6Fe-Cl-Si-KCl samples. Hence, in the air-activated samples, a presence of abundant chloride anions itself does not lead to a formation of iron species in a higher oxidation state.

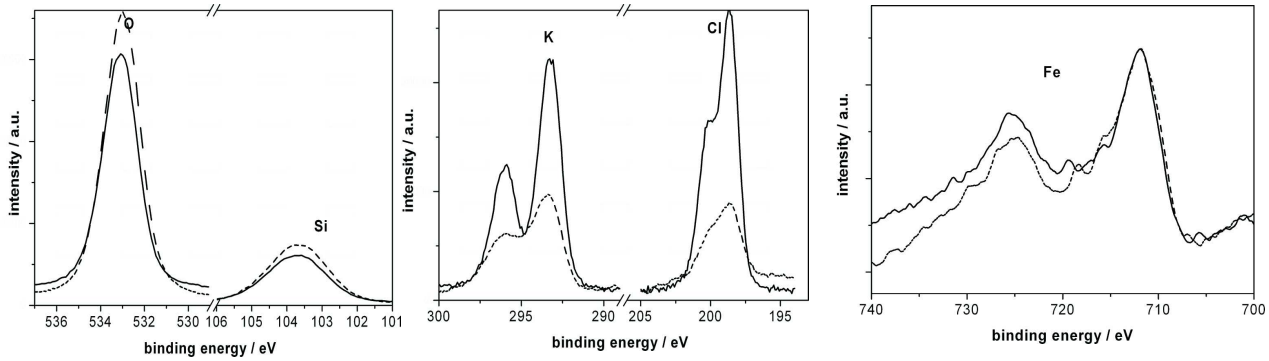

Fig.2.: XPS spectra of the 1Fe-CN-Si (dashed line) and 6Fe-Cl-Si-KCl catalysts (full line). The patterns for K, Cl and Fe were smoothed using a Savitzky-Golay algorithm; the signal for K and Cl for the 1Fe-CN-Si catalyst is multiplied by 10 for better visibility.

For the catalyst 6Fe-Cl-Si-KCl we see a slight increase in the binding energy of oxygen and silicon in comparison to that of the 1Fe-CN-Si sample. Taking in account that the only substantial source of oxygen is SiO_2 and the only substatntial promoter with lower electronegativity is potassium (a cation originating from the potassium ferricyanide precursor), it should indicate an electronic interaction between oxygen in silicon oxide and the potassium promoter. The binding energies of the Fe in the chlorine-rich 6Fe-Cl-Si-KCl and chlorine-lean 1Fe-CN-Si samples seem to be practically the same. Hence, a presence of chlorine does not affect the formal oxidation state of iron, but – as documented by the observation that binding energies of Si and O in chlorine-containing samples are higher by 1.0 and 0.4 eV respectively – attenuates the formation Si-O-K moieties.

To study the interaction between KCl and SiO_2, two modifiactions of the 1Fe-acac-Si-KCl catalyst were prepared: one with an addition of potassium acetate and the second with that of ammonium chloride. Potassium acetate decomposes to potassium oxide upon calcination in air. The addition of KAc (thus enriching the catalyst with potassium) led to a dramatical shifts in the binding energies of K, Si and O, the most conspicious from the above mentioned samples (Fig. 3). Upon addition of KAc – in respect to the NH_4Cl doped samples –, the binding energies decreased from 533.35 to 532.6 eV for O and from 103.85 to 103.4 eV for Si. The binding energy for K increased from 293.0 to 293.50 eV. The value 293.0 eV for K, found in the NH_4Cl-modified sample, is itself slightly above the theoretical value of 292.9 eV for pure

KCl, while 293.5 eV, found in the KAc modified one, indicates a significant change in the surrounding of potassium atom. The K-peak is not only apparently shifted in the KAc-doped sample, and also broadened. (Worth to note that though the maxima of the K-peaks are shifted by 0.5 eV, but both peaks start at the same value, 292 eV.) It necessitates the presence of potassium in two different forms for the KAc-doped sample, one involved in the formation of silicate, and a second one in a form of KCl. A shoulder of O-peak at 530.1 eV for the KAc-doped sample is assigned to oxygen bind to iron.

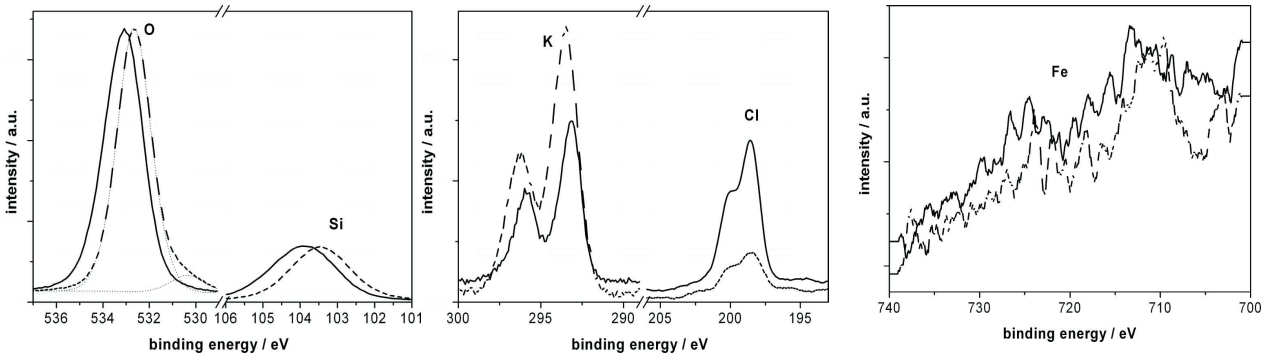

Fig.3.: XPS spectra of the 1Fe-acac-Si-KCl catalyst, prepared by addition of KAc (dashed line) and NH_4Cl (full line) to precursor prior to calcination in air. The patterns for Fe were smoothed using a Savitzky-Golay algorithm.

The above mentioned data indicate that XPS seems to be sufficient to characterize the interactions between Si, O, K and Cl. However, for iron, the results derived from XPS are still unclear. Obviously, the contents of iron in the studied samples is at or near the level of detectability, and the only valid result being derived from the XPS-patterns of iron, is that the atmosphere used during the catalyst calcination seems to be more likely to influence the oxidation state of iron, rather than the presence or absence of chlorine.

3.2 Characterization by N_2O-decomposition

If one assume that iron acts as a redox catalyst, transferring the oxygen atom from N_2O to propylene, two key properties of iron seem to determine its catalytic activity: the redox potential of Fe, and its activity in N_2O decomposition.

Iron-containing active centers are well described for zeolitic materials, a notable application of them being benzene hydroxylation over Fe-ZSM-5 catalysts [28]. These materials, mostly due to their acidic nature, perform poorly in propylene epoxidation. Well-ordered silicalites, due to diffusion problems were found less suitable for epoxidations [23,29]. Hence, in the present case there is a need to characterize the behavior of iron in a less ordered material, where the iron doesn't occupy strictly defined particular positions. (XPS data clearly indicated that there is only a fragment of the overall iron content localized in the most easily accessible positions, near the geometrical surface.) In addition, it is necessary to characterize the fraction of iron, which is practically responsible for the catalytic activity. In analogy with Fe-zeolites, N_2O can be used as a redox probe molecule for supported iron oxide catalysts.

Generally, iron can be present in several oxidation states, in a form of FeO_x agglomerates, oligomeric clusters, or mono- and binuclear species in tetrahedral or octahedral coordination with a various number of Fe-O-Si bridges [30].

The onset of the N_2O decomposition over Fe-zeolites is typically reported above 450°C depending on iron loading and on the nuclearity of Fe species [31]; mononuclear species being determined slightly more active by DFT calculation [32]. In addition α-Fe sites are reported to abstract oxygen atom from N_2O molecule at much lower, even at ambient temperature [27].

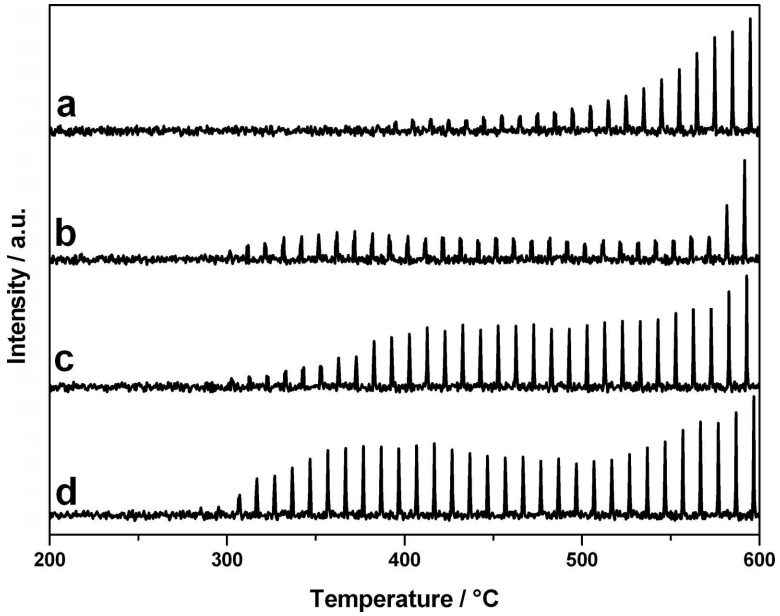

Fig.4.: Pulse N_2O-decomposition patterns for the ion m/z=14 (nitrogen) for catalysts 1Fe-acac-Si-KCl *(N_2)* (**a**), 1Fe-acac-Si-KCl-KAc (**b**), 1Fe-acac-Si-KCl (**c**), 1Fe-acac-Si-KCl-NH_4Cl (**d**). 300 mg of sample, carrier gas 10 $ml.min^{-1}$ helium, N_2O pulse volume 30 µl. Data normalized against the background nitrogen signal.

As seen in Fig.4, the activity of all the tested catalysts in N_2O-decomposition increases rapidly with the increasing temperature in the region near 600 °C, what resembles the activity of Fe-zeolites in N_2O decomposition. However, some samples have a more or less pronounced activity in a temperature region ~300-400 °C. Apparently, a calcination in air, rather than in nitrogen, and a presence of KCl corresponds with the appearence of the inreased activity in N_2O decomposition in a 300-400 °C region.

3.3 TEM characterization

For KCl-doped catalysts, the TEM images clearly show two marked trends: a partial agglomeration of the support SiO_2 particles, and a migration of supported iron oxide particles. The particles of the parent Aerosil support with diameters about 12 nm (Fig. 5a) are agglutinated by the added KCl, which partially covers the surface (fracture planes) of the

agglomerates (Fig. 5b). Apparently, iron oxide nanoparticles, with diameters about 3-20 nm, appear more abundantly in the KCl-rich regions (Fig. 5b) This indicates that one needs to presuppose the surface concentration of iron being dependent on the surface exposition of the KCl.

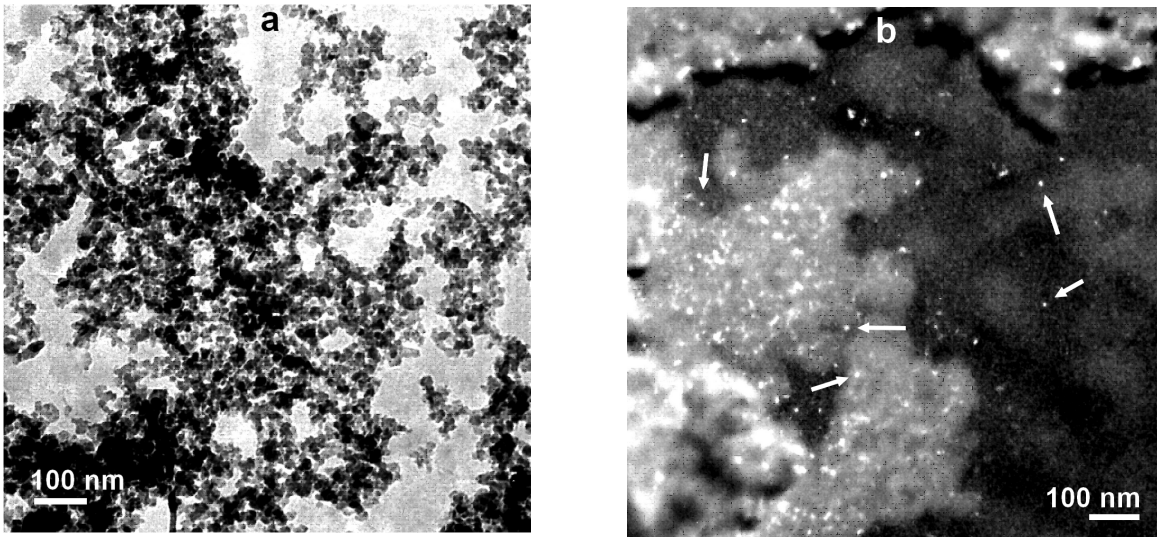

Fig.5.: TEM images of the parent Aerosil support (a), and 1Fe-acac-Si-KCl sample (b).

3.4 Electrochemical characterization

Voltammetric characterization is a sensitive tool to distinguish between redox sites available for the catalytic reaction. The data retrieved from the technique are bulk-specific, hence does not suffer from being representative only for a thin geometrical surface. Moreover, they do provide informations about the crystalline structure of the deposited iron, even at metal loading <1%, hence, bellow the detection limit of XRD techniques.

Four samples, 1Fe-acac-Si-KCl *(N_2)*, 1Fe-acac-Si-KCl-KAc, 1Fe-acac-Si-KCl and 1Fe-acac-Si-KCl-NH_4Cl, were subjected to voltammetric analysis. As seen in Fig. 6, the shapes of the voltammetric patterns for samples 1Fe-acac-Si-KCl *(N_2)* and 1Fe-acac-Si-KCl-KAc are resembling each other, as do for the 1Fe-acac-Si-KCl and 1Fe-acac-Si-KCl-NH_4Cl samples.

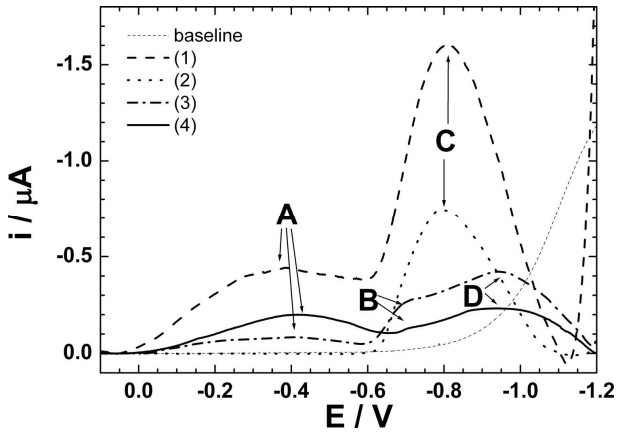

Fig. 6.: Voltammetric patterns of the samples (**1**) - 1Fe-acac-Si-KCl *(N_2)*, (**2**) – 1Fe-acac-Si-KCl-KAc, (**3**) - 1Fe-acac-Si-KCl, (**4**) – 1Fe-acac-Si-KCl-NH_4Cl, measured in an acetate buffer at pH=4.7.

Four peaks could be distinguished in the voltammetric curves of the tested samples, at potentials about -0.4, -0.7, -0.8 and -0.95 V. Isolated iron species are expected to have reduction peaks at the most positive potentials, the theoretical reduction potential of $Fe^{3+}_{(aq)}$ being -0.04V against standard calomel electrode (SCE). Hydrated iron cations in a solution or adsorbed on a solid surface, $[Fe(OH)_x(H_2O)_{6-x}]^{3-x}$, are reported to have reduction signals in the potential region 0.0 to +0.2 V against SCE. The increasing aggregation and crystallinity of iron species is shifting the reduction potential to more negative values. As the reduction potential depends partly also on the particle size of the oxides, and due to a lack of well-defined structure of some iron oxides, especially those with defective or hydrated structure, the attribution of an exact phase structure to a specific potential is hindered by a degree of uncertainty. The reduction signals in the interval 0.0 to -0.4 V are generally assigned to the least ordered iron oxide phases. An amorphous Fe_2O_3 or ferrihydrite precipitate can be associated to reduction maxima in the range -0.1 to -0.2V; a nanocrystalline hematite α-Fe_2O_3 or γ-Fe_2O_3 maghemite is reduced at -0.2 to -0.4 V, finely crystalline hematite at about -0.6 V, well crystalline hematite and maghemite down to -0.9 V. A rare iron oxide form, β-Fe_2O_3 is expected to have reduction potential about -0.4V [25,33].

Fe^{2+} species have reduction potentials usually < -1.0 V, being largely overlapped by the background signal originating from the electrolysis of the acetate buffer used in the voltammetric characterization. However, for the sample 1Fe-acac-Si-KCl *(N_2)* a sharp increase of the reduction current at -1.2 V indicates a presence of Fe^{2+} species.

The absence of reduction peaks in the most electropositive region excludes the formation of isolated iron species in all of the tested catalysts. (For the sample 1Fe-acac-Si-KCl *(N_2)* a very small portion of isolated iron atoms cannot be excluded, represented by a small current at the potential about 0.0 V.) The reduction peak A, at about -0.4 V can be identified as poorly ordered nanocrystalline hematite or maghemite. The formation of such phase is obviously favoured by a calcination in nitrogen. For the samples 1Fe-acac-Si-KCl-KAc, 1Fe-acac-Si-KCl and 1Fe-acac-Si-KCl-NH_4Cl, calcined in air, the intensity of peak A is deteriorated. The extinction of peak A for the sample 1Fe-acac-Si-KCl-KAc is easily explained by a formation of a glass structure caused by the addition of extra potassium, detected also by XPS. Hence the iron oxides with the least ordered crystal structure react the most easily to form an iron-containing glass, undetectable by voltammetry. Samples 1Fe-acac-Si-KCl and 1Fe-acac-Si-KCl-NH_4Cl - both calcined in air– exhibit the reduction peaks at the same potentials, the only significant difference is in the ratio between peak A and the other peaks. This indicates that the addition of extra chlorine to KCl (ammonium chloride in the precursor) does favour the transformation of iron oxides with a more ordered crystal structure, represented by peaks B, C and D into poorly ordered nanocrystalline hematite or maghemite. Peaks B, C and D, at -0.7, -0.8 and -0.95 V represent crystalline iron oxide. Undoubtedly, the reduction potential -0.7 V for peak B clearly lays in the typical potential ranges corresponding to crystalline hematite. Maghemite is expected to have reduction potentials more negative than hematite, at about -0.9 V. This means that peak D should represent crystalline maghemite. Peak C, at -0.8 V laying between the reduction ranges of crystalline hematite and maghemite, can represent either a separated phase, or a kinetically modified form of crystalline hematite or maghemite. This would mean that it is either a more easily reducible maghemite; or it is a kinetically hindered form of hematite. Bearing in mind that a promotion of the iron-containing catalyst by an excess of chlorine led to a less ordered crystalline form of iron, leading to the amplification of the peak A (see sample 1Fe-acac-Si-KCl-NH_4Cl); and also keeping in mind that the peak B occurs in a "glassy" 1Fe-acac-Si-KCl-KAc sample, which is expected to obstruct the reduction of iron

oxide (thus shifting the reduction potentials to more negative values), one should conclude that as an effect of excessive chlorine, the otherwise dominant phase of hematite (peak C) is transformed to poorly ordered nanocrystalline maghemite and hematite, as well as to crystalline maghemite with a typical spinel structure in the 1Fe-acac-Si-KCl and 1Fe-acac-Si-KCl-NH_4Cl samples. The peak B, in the chloride-modified samples thus represents a residual hematite phase. Without chloride addition the hematite phase is represented by the dominant peak C.

3.5 The effect of calcination atmosphere on catalytic properties

For supported iron oxide catalysts using N_2O as an oxidizing agent, a gradual deactivation has been ascribed to a loss of surface oxygen or to coking. Therefore, the activity of the spent catalyst had been reported to be possible to be restored by a burn-off in air [23].

To elucidate the effects of the air treatment at elevated temperature, we calcined the 1Fe-acac-Si-KCl catalyst at 600°C in the flow of air, nitrogen or 5% H_2/N_2, respectively. The performance of catalysts, in terms of PO yields and selectivities, calcined in different atmospheres were clearly different in the first run of the catalytic tests. (Fig. 7). The catalyst calcined in 5% H_2/N_2 mixture exhibited a 1.4% initial PO yield, while the catalyst calcined in air 12.2% PO yield. However, the activity of all three catalysts after 2 h of time on stream (TOS) decreased to rather the same low steady-state level (~ 1% PO yield). In the next reaction-reactivation cycles the activity of catalyst prepared by calcination in air continuously increased and after two reaction-reactivation cycles reached maximal value, which was almost double of the value obtained in the first catalytic run. In the following reaction-reactivation cycles this value (yield of PO about 23.5 mol%) was retained. On the other hand when the catalyst was calcined in nitrogen atmosphere, lower PO yields were achieved. However, in the fifth reaction-reactivation cycle the activity of the nitrogen-calcined catalyst practically reached that of the air-calcined one. The activity of the catalyst calcined in hydrogen atmosphere remained negligible even in the fifth reaction-regeneration cycle.

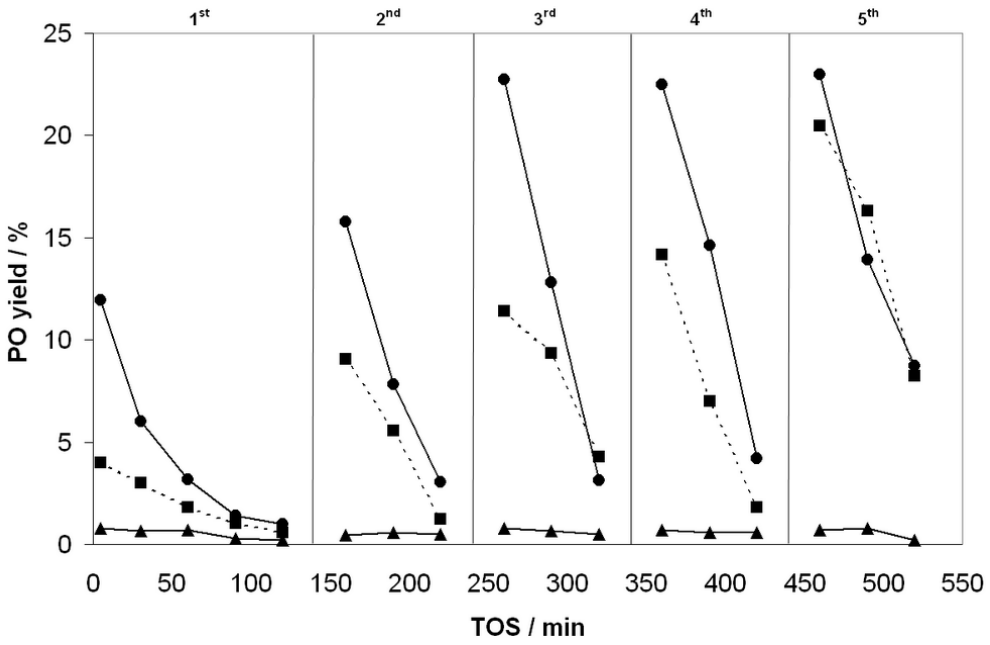

Figure 7.: PO yields of the (●)air-, (■)nitrogen- and (▲)5% H_2/N_2-activated 1Fe-acac-Si-KCl catalysts in five consecutive reaction-regeneration cycles. Reaction temperature: 320 °C, regeneration in air at 600 °C.

3.6 The effect of iron precursor

Depending on the nature of the iron precursor, the epoxidation activity of the iron containing catalysts varies remarkably. In a previous paper it had been shown that catalysts with low iron loading are more selective toward epoxidation, while at higher Fe content the epoxidation activity deteriorated sharply. On the other hand, with the increase of the calcination temperature, it is possible to incorporate higher amount of iron into the silica matrix without losing the epoxidation performance [34]. Here we demonstrate that the presence of an excess of chloride anions or strongly chelating ligands in the iron precursors promote the formation of iron sites bearing high epoxidation activity. Simple iron salts, as nitrate, chloride, formate, as precursors for silica-supported catalysts result in low PO yields, moreover for such iron precursors the increase of iron contents in the catalyst above 0.1% results in a steep decrease in selectivity (Table 1). Organometallic and cyanide complexes allow a deposition of higher

amounts of iron, typically up to 1% without significant decrease of selectivity toward PO. An addition of extra chlorine to $FeCl_3$ precusrsor, in a form of potassium chloride, allowed to increase the iron content in the catalyst up to 5% prior to the propylene combustion begun to dominate over such catalyst. Hence, KCl has similar effect on the amount of incorporated Fe as elevated temperture of calcination.

Table 1: Effect of silica supported iron precursors on catalyst performance at the reaction temperture 320 °C, using N_2O as an oxidizing agent. *Max. PO yield*: a maximal yield observed during a catalytic test, *critical Fe-loading*: a loading above which the PO selectivity dropped bellow 50%.

Precursor	**$Fe(NO_3)_3$**	**Fe(III) formate**	**$K_3[Fe(CN)_6]$**	**$Fe(acac)_3$**	**$Fe(o\text{-}phen)_3$**	**$FeCl_3$ + KCl**	**$FeCl_3$+KCl +NH_4Cl**
Max.PO yield / %	1	1	12	25	28	25	27
Selectivity to PO at 20% conversion	3	5	46	71	73	78	81
Critical Fe loading/ %	<0.1	<0.1	0.1	1	2	5	>5

An addition of ammonium chloride to the KCl promoter – creating a surplus of chlorine relative to potassium in the calcined catalyst – raise further the concentration limit of iron, above which the combustion of propylene started to dominate (>5%). Clearly, the addition of ammonium chloride to KCl led to a cca. 2-fold extension of the catalyst´s lifetime (Fig. 8).

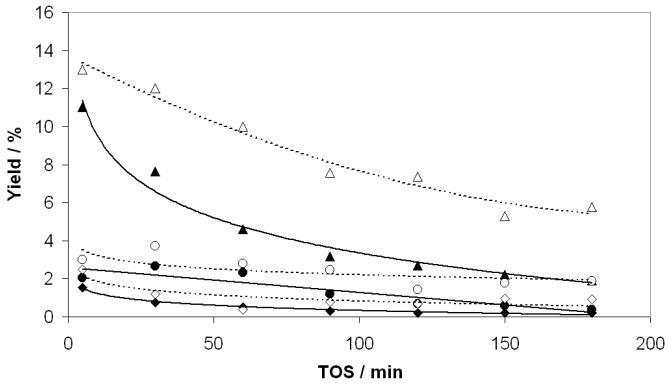

Figure 8: Catalytic performance of the 1Fe-acac-Si-KCl (full symbols) and 1Fe-acac-Si-KCl-NH_4Cl (open symbols) catalysts. ▲-PO, ●-acrolein, ■-CO_2. Reaction temperature: 320 °C.

From among bimetallic catalysts, Fe-Pd, Fe-Cu and Pd-Cu had been tested, along with monometallic Pd- and Cu-based ones. Pd and Cu themselves have been proposed [35,36] for selective epoxidation of olefins, employing a peroxides or molecular oxygen as oxidizing agents. Those metals, however, whether alone or in bimetallic systems, exhibited negligible selectivities to PO (<0.5%) in the current catalytic sytem.

4. Discussion

The specification of iron, finding the catalytically active structures for a particular reaction, and a controlled preparation of such species, is a task contingent on the understanding of several factors.

The disbalance between the overall iron contents in the catalysts and the amount of catalytically active Fe in creation of active oxygen species from N_2O is a well-known phenomenon for Fe-zeolites. The same was found to be true for the FeO_x-KCl/SiO_2 catalysts; in the majority of cases XPS detected only a small portion of iron on the surface (0.4% for the nitrogen activated 1Fe-acac-Si-KCl *(N_2)* sample, and 0.2% for the air-activated one, respectively). Moreover, the air-activated sample with 0.2% surface iron content performed

significantly better in propylene epoxidation in comparison to the nitrogen-activated one with a 0.4% surface Fe content (12.2% PO yield for the air-activated sample, contrary to 4.4% for the nitrogen-actiavted one). These findings, together with the fact that 6Fe-Cl-Si-KCl exhibited practically the same epoxidation activity as the 1Fe-acac-Si-KCl catalyst with 6-fold lower iron content, should mean, that only a certain portion of iron present in the catalyst is active in the epoxidation reaction. That means, as well, that concerning the catalytic activity, there are at least three possible forms of iron present in the catalyst: (i) one portion, responsible for the epoxidation activity in catlysts with low Fe-content and high epoxidation activity (ii) a second one, silent in propylene oxidation, present in catalysts with high Fe-content and high epoxidation activity, (iii) and a third one, present in catalysts with low selectivity in propylene epoxidation.

The disappearance of iron from the visible surface, detected by XPS, possibly explanains why the KCl-doped iron loaded catalysts appear white after calcination. Hence, an addition of potassium chloride, as detected by XPS, has a masking effect on iron. Apart from enhancing the migration of iron, KCl itself migrates from the catalyst´s surface into subsurface layers, remaining less than 10% of the overall content on the surface. Another phenomena, observed for KCl, were its partial decomposition accompanied by a formation of silicates, documented by XPS, and a disbalance in the K/Cl ratio in the calcined samples. This disbalance is in accordance with the formation of silicates: potassium chloride, upon losing chlorine recombines with silicon oxide. A shoulder of O-peak at 530.1 eV in the KAc-doped sample – assigned to Fe-O moietites in a silicate matrix – gives an evidence of the fact, that once a silicate phase is formed, iron oxides can be trapped in. Taking in account that KCl does not affect the oxidation state of the surface iron, as evidenced by XPS, and that in the 1Fe-acac-Si-KCl *(N_2)* sample the transformation of surface SiO_2 into silicates takes place in smaller extent than that of the transformation of KCl, should mean that the formation of silicates and migration of chloride cation must be concurrent dynamic processes. In the oxidizing atmosphere during calcination, the rate of the migration of chlorine to the surface overwhelms the rate of silicate formation. This explains the beneficial effect of extra chlorine, added in the form of ammonium chloride during the preparation step. As it had been shown, potassium chloride tends to migrate from the surface, hence a simultaneous effect of the oxidizing

atmosphere and the abundance of chlorine helps to prevent the iron from being trapped in an inactive silicate matrix.

One of most discussed form of iron in silica-based matrixes is the one associated with α-oxygen, linked to α-Fe^{2+}. A notable property of these sites is their ability to extract the oxygen atom from the N_2O molecule at low, even at ambient temperature; this oxygen atom is then being attainable for a reaction with the organic substrate, again, even at low temperatures. The most crucial question here, keeping in mind that not all Fe^{2+} cations need to be involved in α-sites, is what portion of all Fe^{2+} in the catalyst is in a form of α-Fe^{2+}. Iron in α-sites can be clearly distinguished from other iron species by transition response experiments. An abundance of Fe^{2+} is reportedly formed on iron containing zeolites upon high temperature treatment. The extent of the reduction of the Fe^{3+} depends on the temperature and the atmosphere during the calcination of the catalyst precursor. The Fe^{2+} species generated accordingly, exhibit high initial activity in N_2O decomposition; however they are gradually oxidized by N_2O to inactive Fe^{3+}. These Fe^{2+} sites are not α –sites. The catalytic activity, assigned to α-sites, concerns the portion of iron which retains its ability to decompose N_2O. Moreover, the non- α-Fe^{2+} are deactivated by calcination in the presence of molecular oxygen, while α-sites are reported to not being dependent on such pretreatment [26-28,31]. Hence, α –sites, selective in oxygen insertion into an organic substrate, should survive a certain degree of oxidative treatment, without being overoxidized to an inactive iron moiety. Interestingly, the N_2O-decomposition maxima in the temperature region 300-400 °C were most manifest for the air-activated samples, rather than in nitrogen-activated. In addition, these air-activated catalysts –more active in low-temperature N_2O decomposition – were also most active and selective in propylene epoxidation. Apparently, it cannot be stated that α iron species – observed in Fe-zeolites – are created in an amorphous silica matrix, but the observed data outline an analogous behavior, parallel to α-sites, manifested by an expressed activity in the N_2O decomposition in the case of of the air-activated catalysts.

The voltammetric data show a pronounced transformation of the iron species as a result of the conjunction of the effects of the addition of KCl and a calcination in air flow. Interesting to note that without the presence of air flow during the calcination, the effect of KCl was negligible on the reorganization of the iron oxides. Hence, without an oxidative treatment, the

formation of a crystalline hematite phase dominated, similarly to that of in the KAc-doped sample, accompanied by a formation of silicates.

In the palladium- and copper-modified samples an undesried allylic oxidation of propylene is dominating; most probably copper and palladium are oxidizing propylene separately, with a negligible promoting effect on iron.

5. Conclusions

Propylene can be epoxidized by N_2O with selectivities above 80% over iron-based catalysts. Iron in the form of simple inorganic salts as precursors results in poor epoxidation activity. The main factors leading to a formation of active iron species are mainly a presence of a chelating ligand in the iron precursor, an abundant presence of a chloride anion and oxidative pretreatment of the catalyst. An abundance of chloride allows to increase the iron loading in the catalysts above 5% FeO_X. The best results in propylene epoxidtion were achieved using a FeO_X/SiO_2-KCl catalyst doped with excessive chlorine in a form of an NH_4Cl precursor.

The combination of XPS with electrochemical analysis indicates, that: (i) both KCl and KAc enhances the incorporation of the iron into the silica matrix, thus preventing the formation of large FeO_X agglomerates, detrimental for the selectivity of epoxidation, (ii) the presence of excess Cl prevents the formation of strong electronic interactions between K-Si and Fe-Si, and gives high activity and selectivity in propylene epoxidation, (iii) the catalytic activity correlates with the activity in N_2O decomposition, (iv) the excess chlorine –itself not affecting the oxidation state of iron - favors the formation of poorly crystalline nano-iron oxides.

At least three forms of iron could be distinguished in the catalysts: (i) Fe strongly bound in silicates, inactive in propylene oxidation, (ii) Fe in a form of crystalline hematite, active for undesired side reactions in propylene epoxidation and (iii) Fe species created as the effect of chloride anion and oxidative pretreatment, most probably a crystalline maghemite phase with a spinel structure, formed upon an impact of KCl on the iron species otherwise resulting in a formation of a crystalline hematite phase.

It had been equally shown that iron in the case of studied catalysts does not constitute isolated iron atoms (or at least not in the form being accessible for a redox process), rather there

are nanoparticles of iron active in the epoxidation reaction, with a diameter of 3-20 nm, detected by TEM.

It´s necessary to remark, that the specification of FeO_x on potassium-doped amorphous nano-silica support – e.g. unlike to specification of a zeolitic structure, where the solid framework is strictly determined – is inevitably hindered by various factors, such as the simultaneous formation of several types of amorphous silicates, the contribution of the hydration of the surface, etc. Although, several straightforward findings are presented in this paper, the strict specification of all the interactions between all the components remains a challenge in the case of a rather amorphous catalyst.

6. Acknowledgement

The authors kindly acknowledge a partial financial support from the grant NANOBASE no. CZ1.07/2.3.00/20.0074, and Mr. Peter Bočko from Chemolak Inc. for providing Aerosil samples.

7. References

[1] X. Zheng, Q. Zhang, Y.Guo, W. Zhan, Y. Guo, Y. Wang, G. Lu, J. Mol. Catal. A: Chem., 357 (2012) 106–111.

[2] Z. Suo, M. Jin, J. Lu, Z. Wei, C. Li, J. Nat. Gas Chem. 17 (2008) 184–190.

[3] The Dow Chemical Company, Propylene oxide product sheet, 2013.

[4] T.A. Nijhuis, M. Makkee, J.A. Moulijn, B.M. Weckhuysen, Ind. Eng. Chem. Res., 45 (2006) 3447-3459.

[5] A. C. Kizilkaya, S. Senkab, I. Onal, Journal of Molecular Catalysis A: Chemical, 330 (2010) 107–111.

[6] K. Shen, X.Liu, G. Lu, Y. Miao, Y. Guo, Y. Wang, Y. Guo, Journal of Molecular Catalysis A: Chemical 373 (2013) 78–84.

[7] G. Wu, Y. Wang, L. Wang, W. Feng, H. Shi, Y. Lin, T. Zhang, X. Jin, S. Wang, X. Wu, P. Yao, Chemical Engineering Journal, 215–216 (2013) 306–314.

[8] W. Su, S. Wang, P. Ying, Z. Feng, C. Li, J. Catal., 268 (2009) 165–174.

[9] B. Horváth, T. Soták, M. Hronec, Appl. Cat. A: Gen., 405 (2011)18–24.

[10] A. Held, J. Kowalska-Kuś, A. Łapiński, K. Nowińska, J. of Catal., 306 (2013) 1–10.

[11] S. Hikazudani, T. Mochida, N. Matsuo, K. Nagaoka, T. Ishihara, H. Kobayashi, Y. Takita, J. Mol. Catal. A: Chemical, 358 (2012) 89–98.

[12] T. Liu, P. Hacarlioglu, S. Ted Oyama, M.-F. Luo, X.-R. Pan, J.-Q. Lu, J. Catal., 267 (2009) 202–206.

[13] T. Hayashi, K. Tanaka, M. Haruta, J. Catal., 178 (1998), 566-575.

[14] B. Horváth, M. Hronec, I. Vávra, M. Šustek, Z. Križanová, J. Dérer, E. Dobročka, Catal. Commun. 34 (2013) 16–21.

[15] S. Hikazudani, T. Mochida, N. Matsuo, K. Nagaoka, T. Ishihara, H. Kobayashi, Y. Takita, J. Mol. Catal. A: Chem., 358 (2012) 89–98.

[16] S. Yang, W. Zhu, Q. Zhang, Y. Wang, J. Catal., 254 (2008) 251–262.

[17] Y. Wang, H. Chu, W. Zhu, Q. Zhang, Catal. Today, 131 (2008) 496–504.

[18] L. Yang, J. He, Q. Zhang, Y. Wang, J. Catal., 276 (2010) 76–84.

[19] V.I. Sobolev, A.S. Kharitonov, Ye.A. Paukshtis, G.I. Panov, J. Mol. Cat., 84 (1993) 117–124.

[20] K. Nowinska, A. Waclaw, A. Izbinska, Appl. Catal. A, 243(2003) 225-236.

[21] Y. Wang, K. Otsuka, J. Chem. Soc. Chem, 91 (1995) 3953-3961.

[22] V. Duma, D. Hönicke, J. Catal., 191 (2000) 93–104.

[23] E. Ananieva, A. Reitzmann, Chem. Eng. Sci., 59 (2004) 5509–5517.

[24] B. Horváth, M. Hronec, R. Glaum, Top. Catal., 46 (2007) 129–135.

[25] L. Čapek, V. Kreibich, J. Dědeček, T. Grygar, B. Wichterlová, Z. Sobalík, J.A. Martens, R. Brosius, V. Tokarová, Micropor. Mesopor. Mater. 80 (2005) 279–289.

[26] L. Kiwi-Minsker, D.A. Bulushev, A. Renken, J. Catal. 219 (2003) 273-285.

[27] L.V. Pirutko, V.S. Chernyavsky, A.K. Uriarte, G.I. Panov, Appl. Catal. A 227 (2002) 143–157.

[28] E. V. Starokon, M. V. Parfenov, L. V. Pirutko, I. E. Soshnikov, G. I. Panov, J. Catal. 309 (2014) 453–459.

[29] T. J. Vulic, A. F.K. Reitzmann, K. Lázár, Chem. Eng. J. 207–208 (2012) 913–922.

[30] K. Sun, H.Xia, Z. Feng, R. van Santen, E.Hensen, C. Li, J. Catal. 254 (2008) 383-396.

[31] K.S. Pillai, J.Jia, W.M.H. Sachtler, Appl. Catal. A 364 (2004) 133-139.

[32] N. Hansen, A. Heyden, A.T. Bell, F.J. Keil, J. Catal. 248 (2007) 213-225.

[33] K. Gmucová, M. Weis, V. Nádaždy, I. Capek, A. Šatka, L. Chitu, J. Cirák, E. Majková, Appl. Surf. Sci. 254 (21) (2008) 7008–7013.

[34] B. Horváth, T. Soták, M. Hronec, Appl. Catal. A 405 (2011) 18– 24.

[35] G. Jenzer, T. Mallat, M. Maciejewski, F. Eigenmann, A. Baiker, Appl. Catal. A: General 208 (2001) 125–133.

[36] Y. Wang, H. Chu, W. Zhu, Q. Zhang, Catal. Today 131 (2008) 496–504.